IFIC/12-67

Sneutrino Dark Matter in Low-scale Seesaw Scenarios

Valentina De Romeri* and Martin Hirsch†

AHEP Group, Instituto de Física Corpuscular –

C.S.I.C./Universitat de València Edificio de Institutos de Paterna,

Apartado 22085, E–46071 València, Spain

Abstract

We consider supersymmetric models in which sneutrinos are viable dark matter candidates. These are either simple extensions of the Minimal Supersymmetric Standard Model with additional singlet superfields, such as the inverse or linear seesaw, or a model with an additional U(1) group. All of these models can accomodate the observed small neutrino masses and large mixings. We investigate the properties of sneutrinos as dark matter candidates in these scenarios. We check for phenomenological bounds, such as correct relic abundance, consistency with direct detection cross section limits and laboratory constraints, among others lepton flavour violating (LFV) charged lepton decays. While inverse and linear seesaw lead to different results for LFV, both models have very similar dark matter phenomenology, consistent with all experimental bounds. The extended gauge model shows some additional and peculiar features due to the presence of an extra gauge boson Z' and an additional light Higgs. Specifically, we point out that for sneutrino LSPs there is a strong constraint on the mass of the Z' due to the experimental bounds on the direct detecton scattering cross section.

*Electronic address: deromeri@ific.uv.es

†Electronic address: mahirsch@ific.uv.es

I. INTRODUCTION

Although the existence of dark matter (DM) is supported by a variety of astrophysical data, its identity is unknown. Many particle physics candidates have been proposed to explain the DM [1]. In supersymmetric extensions of the standard model (SM) there are the lightest neutralino and the scalar neutrino, which could both provide the correct relic density for the DM [2]. The neutralino as a DM candidate has been studied in literally hundreds of publications, but also sneutrinos as candidates for the cold dark matter have actually quite a long history [3–5]. However, ordinary left sneutrinos, i.e. the sneutrinos of the MSSM (Minimal Supersymmetric Extension of the SM), have been ruled out [6] as the dominant component of the dark matter in the galaxy a long time ago due to their large direct detection cross section [7]. This leaves only "mixed" sneutrinos, i.e. sneutrinos which are partly singlets under the SM group, as good DM candidates. Motivated by neutrino oscillation data [8], in this paper we study scalar neutrinos as DM candidates in models with a low-scale seesaw mechanism, either MSSM-like models with an inverse [9] or the linear seesaw [10, 11] or models based on an $U(1)_{B-L} \times U(1)_R$ extension of the MSSM group [12, 13].

Singlet sneutrinos as DM have been studied in the literature before. Neutrino masses require that pure Dirac sneutrino must have tiny Yukawa couplings. Unless the trilinear parameters are huge, Dirac (right) sneutrinos are therefore never in thermal equilibrium in the early universe [14, 15]. [1] However, they could still be non-thermal DM produced in the decay of the NLSP ("next-to-lightest supersymmetric particle") [18]. Also, trilinear terms are usually thought to be proportional to the associated Yukawa couplings, $T_\nu \propto Y_\nu A \sim \mathcal{O}(1)$ eV. Treating T_ν as a free parameter of the order of $\mathcal{O}(100)$ GeV, Dirac sneutrinos can be made good thermal DM candidates, as has been discussed in [19–21]. Very light mixed sneutrinos of this type have been studied in [22]. The LHC phenomenology of mixed Dirac sneutrino DM was studied in [23]. Alternatively to a large A-term, Dirac sneutrinos could also be made thermal DM in models with an extended gauge group [24, 25].

In the classical seesaw picture [26–29] lepton number is broken at a very large energy

[1] Unless Dirac neutrino masses are due to a tiny vev of a non-standard Higgs field [16]. In this case, Dirac sneutrinos could be the DM and even explain the much discussed claim for a tentative 130 GeV γ line in the FERMI data [17].

scale, possibly close to the unification scale. In such a setup also the right sneutrinos are very heavy and decouple; the sneutrinos remaining in the light spectrum are then very MSSM-like. One could, of course, simply put the scale of the seesaw low, say around the TeV scale. Yukawa couplings of the order of $\mathcal{O}(10^{-6})$ could fit neutrino data and the right sneutrinos are thermalized. In such an electro-weak scale seesaw right sneutrinos are overabundant unless (i) (again) a large trilinear parameter is assumed [30]; (ii) a new $U(1)$ group is introduced [31]; or (iii) sneutrinos have a large coupling to the NMSSM ("next-to-minimal Supersymmetric Standard Model") singlet [32, 33].

However, the situation is different in extended seesaw schemes like the inverse [9] or the linear seesaw [10, 11]. Here, additional singlets need to be introduced, but the neutrino Dirac Yukawa couplings can take essentially any value and it is the smallness of the inverse or linear seesaw terms which "explains" the smallness of the observed neutrino masses. In these setups the sneutrinos are highly mixed states. Inverse seesaw sneutrino DM has been studied previously in [34, 35]. Our work differs in several aspects from these earlier papers. [34] calculated all masses at tree-level and did not carry out a detailed fit to neutrino data, while we use full 2-loop RGEs for the parameters, one-loop corrected mass matrices and pay special attention to constraints from neutrino masses. Also the paper [35] has some overlap with our work, but concentrates more on collider phenomenology of the inverse seesaw with sneutrino DM.

There are also some recent paper studying extended gauge groups. [36] studies inverse seesaw in an $SU(2)_R$ extension of the MSSM. Also two papers based on sneutrinos in $U_{B-L}(1) \times U_Y(1)$ have been published recently. In [37] an inverse seesaw is implemented in $U_{B-L}(1) \times U_Y(1)$. In [38] sneutrino DM within the $U_{B-L}(1) \times U_Y(1)$ group was studied assuming a standard seesaw. However, none of the above papers has studied linear seesaw variants. Finally, we mention that part of the results discussed in this paper have been presented previously at conferences [39].

All our numerical calculations have been done using `SPheno` [40, 41], for which the necessary subroutines were generated using the package `SARAH` [42–44]. We have written the SARAH input files for the inverse and the linear seesaw, while for the $U(1)_{B-L} \times U(1)_R$ model we used the SARAH input files from [13]. The calculation of the relic density of the LSP is then done with `MicrOmegas` [45] version `2.4.5` based on the `CalcHep` [46] output of `SARAH`. To perform the scans we used a Mathematica package (`SSP`) [47].

The rest of this paper is organized as follows. In the next section we first recall the main features of the supersymmetric inverse and linear seesaws, before discussing briefly the minimal $U(1)_{B-L} \times U(1)_R$ extension of the standard model. In section (III) we discuss phenomenological constraints on the parameter space of the different setups. In section (IV) we then calculate the relic density and direct detection cross section. We conclude in section (V).

II. SETUP: LOW SCALE SEESAWS AND EXTENDED GAUGE GROUPS

In this section we briefly discuss the different setups, which we will use in the numerical sections of the paper. We first discuss supersymmetric inverse and linear seesaw, before recalling the main features of the minimal $U(1)_{B-L} \times U(1)_R$ extension of the MSSM. The latter can be realized with either inverse or linear seesaw, but has some interesting additional features which are not covered by either the inverse or linear seesaw extensions of the MSSM.

A. Inverse and linear seesaw

In both, the inverse and the linear seesaws the particle content of the MSSM is extended by two types of singlet superfields, $\hat{\nu}^c$ and $\hat{S}$. The former is assigned a $L = +1$, while the latter has formally $L = -1$. The total superpotential can be written as

$$W = W_{\rm MSSM} + W_{\nu^c} + W_{\rm ISS} + W_{\rm LSS} \tag{1}$$

Here, $W_{\rm MSSM}$ is the usual MSSM superpotential

$$W_{\rm MSSM} = Y_u \, \hat{u} \, \hat{q} \, \hat{H}_u \, - Y_d \, \hat{d} \, \hat{q} \, \hat{H}_d \, - Y_e \, \hat{e}^c \, \hat{l} \, \hat{H}_d \, + \mu \, \hat{H}_u \, \hat{H}_d \; . \tag{2}$$

Lepton number conserving terms for the new singlet fields $\hat{\nu}^c$ ("right-handed neutrino") and $\hat{S}$ can be written as

$$W_{\nu^c} = Y_\nu \, \hat{\nu}^c \, \hat{l} \, \hat{H}_u \, + M_R \, \hat{\nu}^c \, \hat{S} \; . \tag{3}$$

The first term generates Dirac neutrino masses, once the H_u acquires a vacuum expectation value, while the second term is a mass term for the new singlet fields. In the inverse seesaw lepton number is violated by the term

$$W_{\rm ISS} = \frac{1}{2} \mu_S \, \hat{S} \, \hat{S} \; , \tag{4}$$

while in the linear seesaw case one writes lepton number violation as:

$$W_{\rm LSS} = Y_{SL}\, \hat{S}\, \hat{l}\, \hat{H}_u \ . \tag{5}$$

In both cases, it is usually assumed that the lepton number violating terms are small [9–11], see also the discussion in section (III). The neutrino mass matrix and the resulting constraints on the model parameters are discussed in section (III A).

In supersymmetric models with lepton number violation, also the scalar neutrinos must have a lepton number violating mass term [48]. This term, $\tilde{m}^2_M$, is given by the difference between the eigenvalues of the real and imaginary components of the scalar neutrinos. It is therefore convenient to separate the sneutrino mass matrix into CP-even and CP-odd blocks [49]: [2]

$$\mathcal{M}^2 = \begin{pmatrix} \mathcal{M}^2_+ & \mathbf{0} \\ \mathbf{0} & \mathcal{M}^2_- \end{pmatrix} . \tag{6}$$

Mass matrices for the scalar neutrinos are different in the inverse and linear seesaws. At the tree-level, in the inverse seesaw the $\mathcal{M}^2_\pm$ are given by: [3]

$$\mathcal{M}^2_{\pm,ISS} = \begin{pmatrix} m_L^2 + D^2 + (m_D^T m_D) & A_{LR}^T & m_D^T M_R \\ A_{LR} & m^2_{\nu^c} + (M_R M_R^T) + (m_D m_D^T) & \pm M_R \mu_S + B_{M_R} \\ M_R^T m_D & \pm \mu_S M_R^T + B^T_{M_R} & m_S^2 + \mu_S^2 + M_R^T M_R \pm B_{\mu_S} \end{pmatrix} \tag{7}$$

Here, $D^2 = \frac{1}{2} m_Z^2 \cos 2\beta$ are the MSSM D-terms, $m_D = \frac{1}{\sqrt{2}} v_u Y_\nu$, $A_{LR} = T_{Y_\nu} v_u - \mu m_D \mathrm{cotg}\beta$, B_{M_R} is the soft bilinear term, T_{Y_ν} is the soft trilinear and m_L^2, $m^2_{\nu^c}$ and m_S^2 are the scalar soft masses for the doublet and the singlets respectively. Only μ_S and the corresponding bilinear soft term B_{μ_S} violate lepton number and only these two come with different signs in the CP-even and CP-odd mass matrices.

For the linear seesaw one finds

$$\mathcal{M}^2_{\pm,LSS} = \begin{pmatrix} m_L^2 + D^2 + (m_D^T m_D) + (M_L^T M_L) & A_{LR}^T \pm M_L^T M_R^T & m_D^T M_R \pm A_{LS}^T \\ A_{LR} \pm M_R M_L & m^2_{\nu^c} + (M_R M_R^T) + (m_D m_D^T) & \pm m_D M_L^T + B_{M_R} \\ M_R^T m_D \pm A_{LS} & \pm M_L m_D^T + B^T_{M_R} & m_S^2 + M_L M_L^T + M_R^T M_R \end{pmatrix} \tag{8}$$

[2] Separation into CP-even and CP-odd blocks requires CP-conservation, i.e. all parameters in the mass matrices below have to be real.

[3] We correct some misprints in [34, 69]

with all definitions as in eq. (7) and $M_L = \frac{1}{\sqrt{2}} v_u Y_{SL}$ and $A_{LS} = T_{Y_{SL}} v_u - \mu M_L \mathrm{cotg}\beta$. In these simple setups all other mass matrices are as in the MSSM and, therefore, not discussed here.

B. Minimal $SU(3)_c \times SU(2)_L \times U(1)_{B-L} \times U(1)_R$ extension of the MSSM

In order to explain why neutrinos are so much lighter than all other matter particles, we have considered in the previous section two variants of the seesaw which can, in principle, be implemented at virtually any mass scale. Such seesaw schemes are actually most easily realized in a particular class of extensions of the MSSM with an extended gauge group [50–52] based on the $SO(10)$ breaking chains

$$SO(10) \rightarrow SU(3)_c \times SU(2)_L \times SU(2)_R \times U(1)_{B-L} \rightarrow SU(3)_c \times SU(2)_L \times U(1)_Y \quad (9)$$

$$\begin{aligned} SO(10) &\rightarrow SU(3)_c \times SU(2)_L \times SU(2)_R \times U(1)_{B-L} \quad (10) \\ &\rightarrow SU(3)_c \times SU(2)_L \times U(1)_R \times U(1)_{B-L} \rightarrow SU(3)_c \times SU(2)_L \times U(1)_Y \end{aligned}$$

A MSSM-like gauge unification is in this case perfectly viable, and compatible with a $U(1)_R \times U(1)_{B-L}$ stage stretching down to TeV. We will follow eq. (10), since this variant can be realized with the minimal number of additional superfields with respect to the MSSM particle content. This model [50, 52], which we will call the minimal $U(1)_{B-L} \times U(1)_R$ extension (mBLR, for short) has been studied in two recent papers [12, 13]. We will follow the notation of [13] quite closely.

The particle content of the mBLR model is given in table (I). In this setup, the presence of $\hat{\nu}^c$ is required for anomaly cancellation. Breaking the $SU(2)_L \times U(1)_{B-L} \times U(1)_R$ to $U(1)_Q$ requires additional Higgs fields. The vev of the fields χ_R and $\bar{\chi}_R$ break $U(1)_{B-L} \times U(1)_R$, while the vevs of H_u and H_d break $SU(2)_L$ and $U(1)_Y$. Note that since H_u and H_d are charged also under $U(1)_R$, in the mBLR new D-terms are generated in the mass matrix for the scalars. These additional contributions with respect to the MSSM allow to have a larger mass for the lightest MSSM-like CP-even mass eigenstates and makes it possible to have a $m_{h^0} \simeq 125$ GeV without constraints on the supersymmetric particle spectrum [12, 13].

Assuming matter parity [13], apart from the MSSM superpotential the model also has the terms

$$W_S = Y_\nu \hat{\nu^c} \hat{L} \hat{H}_u + Y_s \hat{\nu^c} \hat{\chi}_R \hat{S} - \mu_R \hat{\bar{\chi}}_R \hat{\chi}_R + \mu_S \hat{S} \hat{S}. \quad (11)$$

	Superfield	$SU(3)_c \times SU(2)_L \times U(1)_R \times U(1)_{B-L}$	Generations
	$\hat{Q}$	$(\mathbf{3}, \mathbf{2}, 0, +\frac{1}{6})$	3
	$\hat{d^c}$	$(\overline{\mathbf{3}}, \mathbf{1}, +\frac{1}{2}, -\frac{1}{6})$	3
	$\hat{u^c}$	$(\overline{\mathbf{3}}, \mathbf{1}, -\frac{1}{2}, -\frac{1}{6})$	3
	$\hat{L}$	$(\mathbf{1}, \mathbf{2}, 0, -\frac{1}{2})$	3
	$\hat{e^c}$	$(\mathbf{1}, \mathbf{1}, +\frac{1}{2}, +\frac{1}{2})$	3
	$\hat{\nu^c}$	$(\mathbf{1}, \mathbf{1}, -\frac{1}{2}, +\frac{1}{2})$	3
	$\hat{S}$	$(\mathbf{1}, \mathbf{1}, 0, 0)$	3
	$\hat{H}_u$	$(\mathbf{1}, \mathbf{2}, +\frac{1}{2}, 0)$	1
	$\hat{H}_d$	$(\mathbf{1}, \mathbf{2}, -\frac{1}{2}, 0)$	1
	$\hat{\chi}_R$	$(\mathbf{1}, \mathbf{1}, +\frac{1}{2}, -\frac{1}{2})$	1
	$\hat{\bar{\chi}}_R$	$(\mathbf{1}, \mathbf{1}, -\frac{1}{2}, +\frac{1}{2})$	1

TABLE I: The Matter and Higgs sector field content of the $U(1)_R \times U(1)_{B-L}$ model. Generation indices have been suppressed. The $\hat{S}$ superfields are included to generate neutrino masses via the inverse seesaw mechanism. Under matter parity, the matter fields are odd while the Higgses are even.

The 2nd term generates $M_R = \frac{1}{\sqrt{2}} Y_s v_{\chi_R}$ while the last term generates the inverse seesaw discussed above. The model can, in principle, also be written with a linear seesaw included [50]. Note, that the model assigns lepton number necessarily in a different way then discussed in the last subsection, since here $B-L$ is gauged. Thus, $B-L$ is broken by the vevs of χ_R and $\bar{\chi}_R$. However, neutrino masses are generated in exactly the same way as in the simpler inverse seesaw model, discussed in the previous subsection.

It is useful to reparametrize the vevs in a notation similar to the MSSM, i.e.:

$$v_R^2 = v_{\chi_R}^2 + v_{\bar{\chi}_R}^2 \ , \quad v^2 = v_d^2 + v_u^2 \qquad (12)$$
$$\tan\beta_R = \frac{v_{\chi_R}}{v_{\bar{\chi}_R}} \ , \quad \tan\beta = \frac{v_u}{v_d}.$$

The mass of the new Z'-boson is approximately given by [13]

$$m_{Z'}^2 = \frac{g_R^4 v^2}{4(g_{BL}^2 + g_R^2)} + \frac{1}{4}(g_{BL}^2 + g_R^2) v_R^2 \, . \qquad (13)$$

Thus, v_R must be larger than approximately $v_R \gtrsim 5$ TeV, see also next section.

Mass matrices for all sfermions for this model can be found in [13]. For us the sneutrino mass matrix is most important. In the mBLR model it is given by the expression for the inverse seesaw, with exception of $M_R = \frac{1}{\sqrt{2}} Y_s v_{\chi_R}$ and new D-term contributions:

$$\begin{aligned} D^2_{LL} &= \tfrac{1}{8} \left((g^2_{BL} + g^2_{BLR} - g_{BL} g_{RBL}) v^2_R \cos(2\beta_R) + (g^2_L + g^2_R + g_{BL} g_{RBL}) v^2 \cos 2\beta \right) \\ D^2_{RR} &= \tfrac{1}{8} \Big((g^2_{BL} + g^2_R + g^2_{BLR} + g^2_{RBL} - 2 g_{BL} g_{RBL} - 2 g_R g_{BLR}) v^2_R \cos(2\beta_R) \\ &\quad + (g^2_R + g^2_{RBL} - g_{BL} g_{RBL} - g_R g_{BLR}) v^2 \cos 2\beta \Big) \end{aligned} \tag{14}$$

Here, D^2_{LL} replaces D^2 of the simpler models, while D^2_{RR} are the new D-terms in the $(\tilde{\nu}^c, \tilde{\nu}^c)$ part of the mass matrix. Due to the lower limit for the Z' mass, see eq. (13), and since the new D-terms in eq. (14) can have either sign, the free parameter $\tan\beta_R$ is constrained to be close to $\tan\beta_R \simeq 1$, otherwise either one of the sneutrinos (or one of the charged sleptons) becomes tachyonic.

III. PHENOMENOLOGICAL CONSTRAINTS

In this section we discuss phenomenological constraints on the parameter space of the different models. Below, we concentrate on neutrino masses and lepton flavour violation. Other constraints on the model space come from SUSY searches at colliders, from Z^0 physics (LEP) and from the Higgs results of the LHC collaborations ATLAS [53] and CMS [54].

"Heavy" singlet neutrinos with mass below the Z^0 boson are excluded by LEP experiments [55], which set limits on $|U^\nu_{ij}|^2$ of the order of 10^{-3} to 10^{-5} for the neutrino mass range from 3 GeV up to 80 GeV. L3 has searched also for heavy iso-singlet neutrinos decaying via $N \to lW$ and set limits which range from $|U^\nu_{ij}|^2 \lesssim 2 \times 10^{-3}$ for masses of 80 GeV to $|U^\nu_{ij}|^2 \lesssim 10^{-1}$ for masses of 200 GeV [56]. Most importantly, the invisible width of the Z^0 boson [57] puts an upper limit on the 3×3 sub-block U^ν_{ij}, $i, j \leq 3$, of the neutrino mixing matrix: $\left| 1 - \sum_{ij=1, i \leq j}^{3} \left| \sum_{k=1}^{3} U^\nu_{ik} U^{\nu,*}_{jk} \right|^2 \right| < 0.009$ at the 3-σ level even in the case that the new mostly singlet neutrinos are heavier than the Z^0 boson [13]. Finally, the Z^0 width rules out pure left sneutrinos lighter than approximately half of the Z^0 mass, but sneutrinos with suppressed coupling to the Z^0 below roughly $0.02 - 0.1$ with respect to the MSSM coupling and masses below $m_{\tilde{\nu}} \lesssim 40$ GeV are allowed.

In inverse seesaw models the Higgs can decay to heavy plus light neutrino, if the heavy neutrino has a mass below the Higgs mass [13, 58]. This limits the Yukawa couplings

to roughly below $|Y_\nu| \lesssim 0.02$ for $M_R \lesssim 120$ GeV from measured data on the channel $h \to WW^* \to ll\nu\nu$ [58]. For larger masses current Higgs searches provide essentially no constraint yet.

For the model with the extended gauge group searches for a new Z' boson at the LHC provide important constraints. Both, CMS [59] and ATLAS [60] have searched for, but not observed any hints for, Z''s within the context of different models. For the $U(1)_{B-L} \times U(1)_R$ model the limits are of the order of (roughly) $m_{Z'} \gtrsim (1.7 - 1.8)$ TeV.

SUSY searches at ATLAS [61] and CMS [62] provide lower limits on squark and gluino masses. For example, in mSUGRA/CMSSM models with $\tan\beta = 10$, $A_0 = 0$ and $\mu > 0$, squarks and gluinos of equal mass are excluded for masses below 1500 GeV [61]. This limit essentially rules out any value of $M_{1/2}$ below approximately $(600 - 700)$ GeV for $m_0 \lesssim 1000$ GeV and $M_{1/2}$ below $(350 - 400)$ GeV in the limit of large m_0 for pure CMSSM. Of course, the observation of a new resonance with a mass around $125 - 126$ GeV [53, 54], if interpreted as the lightest Higgs boson, provides important constraints on SUSY parameters as well. However, these constraints are different for the different models we study in this paper. We will discuss them therefore when we discuss numerical scans in section (IV).

A. Neutrino masses

1. *Inverse seesaw*

In the inverse seesaw the neutrino mass matrix can be written at tree-level as

$$M^\nu = \begin{pmatrix} 0 & m_D^T & 0 \\ m_D & 0 & M_R \\ 0 & M_R^T & \mu_S \end{pmatrix}, \tag{15}$$

The smallness of the observed neutrino masses is then usually explained as the hierarchy $\mu_S \ll m_D < M_R$.

Following the notation of [63], we can count the number of physical parameters of the model as $N_{\rm phys} = N_Y - N_G + N_{G'}$. Here, N_Y is the number of parameters in the Yukawa matrices (or mass matrices), G is the original symmetry group which is broken into G' by the presence of the Yukawas (or mass terms). In table II the counting for the inverse seesaw is summarized.

	Parameters	Moduli	Phases
N_Y	Y_e, Y_ν, M_R Dirac type	$3 \times n^2$	$3 \times n^2$
N_Y	μ_S Majorana type	$\frac{n(n+1)}{2}$	$\frac{n(n+1)}{2}$
G	$U(n)_L \bigotimes U(n)_{\nu^c} \bigotimes U(n)_{e^c} \bigotimes U(n)_S$	$4 \times \frac{n(n-1)}{2}$	$4 \times \frac{n(n+1)}{2}$
G'	no LF conservation		
N_{phys}		21	9

TABLE II: Parameter counting for MSSM with an inverse seesaw for three generations.

After absorbing all unphysical parameters by field rotations, we find a total of 30 real parameters, 21 moduli (12 masses and 9 mixing angles) plus 9 phases. It is common practice to choose a basis in which the charged lepton mass matrix (Yukawa: Y_e) is diagonal, which fixes 3 parameters. The remaining parameters could be fixed by going to a basis where M_R is real and diagonal. In this case Y_ν and μ_S are completely general, arbitrary matrices, containing the remaining 24 free parameters. For fitting the neutrino data, however, it is more useful to first rewrite the neutrino Yukawa couplings using a generalization of the Casas-Ibarra parametrization [64].

Consider first the effective mass matrix of the light neutrinos for the inverse seesaw. It is given by

$$m_\nu^{eff} = m_D^T M_R^{T^{-1}} \mu_S M_R^{-1} m_D, \tag{16}$$

We can rewrite m_D as [65]

$$m_D = M_R^T V_\mu^T (\sqrt{\hat{\mu}_S})^{-1} R \mathrm{Diag}(\sqrt{m_{\nu_i}}) U_\nu. \tag{17}$$

Here U_ν is the mixing matrix determined by the oscillation experiments, in the basis where the charged lepton mass matrix is diagonal, m_{ν_i} are the three light neutrino masses, R is an arbitrary real orthogonal 3×3 matrix and $\hat{\mu}_S$ are the eigenvalues of the matrix μ_S with V_μ the matrix which diagonalizes μ_S.

Eqs (16) and (17) allow to fit neutrino data in a straightforward way, if the tree-level contribution dominates, see below. Since one can always choose a basis where M_R is diagonal,

the flavour violation necessary to fit oscillation data resides in m_D and in μ_S. Particularly simple solutions are found, assuming either μ_S or m_D are diagonal too. For diagonal μ_S, for example, one finds

$$m_D = \mathrm{Diag}(\sqrt{\frac{m_{\nu_i}}{\mu_{S_i}}} M_{R_i}) U_\nu . \tag{18}$$

Oscillation experiments have determined the mass squared differences and mixing angles of the active neutrinos with high precision, see for example [8]. Recently also the last of the mixing angles in the left-handed neutrino sector has been measured in two reactor neutrino experiments, DAYA-BAY [66] and RENO [67]. With all these data, the situation can be summarized as follows: The atmospheric neutrino mass squared difference and angles are $\Delta(m^2_{\rm Atm}) = (2.31 - 2.74) \times 10^{-3}$ eV^2 (normal hierarchy) and $\sin^2\theta_{\rm Atm} = 0.36 - 0.68$, the solar parameters are $\Delta(m^2_\odot) = (7.12 - 8.20) \times 10^{-5}$ eV^2 and $\sin^2\theta_\odot = 0.27 - 0.37$ and finally $\sin^2\theta_{13} = 0.017 - 0.033$, all at 3 σ c.l. [8]. Apart from the data on the reactor angle, neutrino angles are still well-fitted by the tribimaximal mixing ansatz [68], which has $\sin^2\theta_{\rm Atm} = 1/2$ and $\sin^2\theta_\odot = 1/3$.

The large atmospheric and solar angles require large off-diagonals in at least one of the two matrices Y_ν or μ_S. For the case of strict normal hierarchy ($m_{\nu_1} \equiv 0$) and diagonal μ_S, oscillation data can be well fitted to leading order in the small parameter $\sin\theta_{13}$ by

$$Y_\nu = |Y_\nu| \begin{pmatrix} 0 & 0 & 0 \\ a & a(1 - \frac{\sin\theta_{13}}{\sqrt{2}}) & -a(1 + \frac{\sin\theta_{13}}{\sqrt{2}}) \\ \sqrt{2}\sin\theta_{13} & 1 & 1 \end{pmatrix} , \tag{19}$$

with

$$a = \left(\Delta m^2_\odot / \Delta m^2_{\rm Atm}\right)^{\frac{1}{4}} \sim 0.4 , \tag{20}$$

where $|Y_\nu|$ can be easily calculated from μ_S and M_R.

The above discussion is valid at tree-level. In the inverse seesaw neutrino masses also receive important corrections at the 1-loop level, once B_{μ_S} becomes sizeable [69]. An example is shown in fig. (1). Here, we have chosen as an example $m_0 = 100$, $M_{1/2} = 1000$, $A_0 = 0$ (all in GeV) $\tan\beta = 10$, $\mathrm{sgn}(\mu) > 0$ and $M_R = 250$ GeV. For this plot we assume μ_S and $B_{M_R} = 3 \times 10^4$ GeV^2 to be diagonal and degenerate. Y_ν is then fitted by eq.(17). A smaller value of μ_S implies then a larger value for the entries in Y_ν.

In the left of fig. (1) we show m_{ν_2} and m_{ν_3} as function of B_{μ_S}, while the plot on the right shows the same neutrino masses as a function of $m^2_{\tilde{M}}$, the mass squared difference

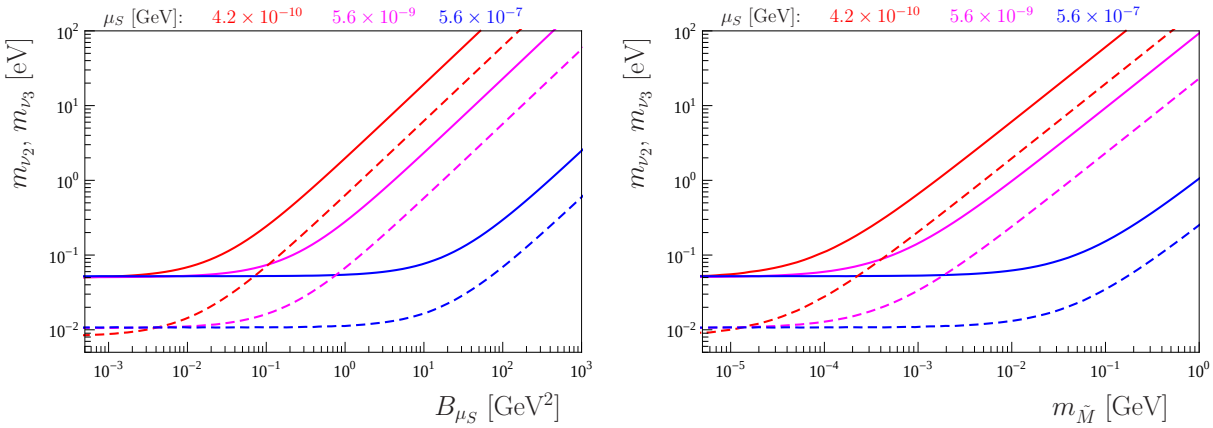

FIG. 1: Neutrino masses versus B_{μ_S} (left) and versus $m_{\tilde{M}}$ (right) for one particular but arbitrary parameter point (see text), for three different values of μ_S.

between the CP-even and CP-odd sneutrinos. This splitting is proportional to B_{μ_S}, while loop neutrino masses are proportional to $Y_\nu^2 B_{\mu_S}$. To restrict the neutrino mass to be smaller than the atmospheric scale than results in an upper limit on $Y_\nu^2 B_{\mu_S}$. For $|\mu_S| \sim 5 \times 10^{-7}$ GeV, corresponding to the largest entries in Y_ν to be of order $\mathcal{O}(10^{-2})$, the splitting can be as large as $\mathcal{O}(10^{-1})$ GeV. Note, however, that with typical mSugra-like boundary conditions one expects naively that $B_{\mu_S} \simeq \mu_S m_0 \sim 10^{-4} - 10^{-7}$ GeV^2. In this case splitting between the sneutrinos becomes negligible.

2. *Linear seesaw*

For the linear seesaw the neutrino mass matrix is given by

$$M^\nu = \begin{pmatrix} 0 & m_D^T & M_L^T \\ m_D & 0 & M_R \\ M_L & M_R^T & 0 \end{pmatrix}, \tag{21}$$

with the effective neutrino mass matrix for the light neutrinos given as

$$m_\nu = m_D^T M_R^{T^{-1}} M_L + M_L^T M_R^{-1} m_D. \tag{22}$$

For the linear seesaw one finds for the CI parametrization [65]

$$m_D = -M_R (M_L^T)^{-1} U_\nu^T \sqrt{m_{\nu_i}} A \sqrt{m_{\nu_i}} U_\nu \tag{23}$$

where A has the following general form:

$$\begin{pmatrix} \frac{1}{2} & a & b \\ -a & \frac{1}{2} & c \\ -b & -c & \frac{1}{2} \end{pmatrix}, \tag{24}$$

with a, b, c real, but arbitrary numbers. The parameter counting for the linear seesaw is given in table (III). We have in total 36 real parameters, 24 moduli (12 masses and 12 mixing angles) plus 12 phases. Fits to neutrino data can be easily done using eqs (22) and (23).

For example, for strict normal hierarchy, degenerate M_R and diagonal and degenerate Y_{SL} one finds to leading order in θ_{13}

$$\begin{aligned} Y_\nu = |Y_\nu|\{ \; - \; \frac{m_{\rm Atm}}{2} & \begin{pmatrix} 0 & \frac{\sin\theta_{13}}{\sqrt{2}} & \frac{\sin\theta_{13}}{\sqrt{2}} \\ \frac{\sin\theta_{13}}{\sqrt{2}} & \frac{1}{2} & \frac{1}{2} \\ \frac{\sin\theta_{13}}{\sqrt{2}} & \frac{1}{2} & \frac{1}{2} \end{pmatrix} \\ + \; \frac{m_\odot}{3} \times \Big(& \begin{pmatrix} -1 & -1 & 1 \\ -1 & -1 & 1 \\ 1 & 1 & -1 \end{pmatrix} + \sqrt{2}\sin\theta_{13} \times \begin{pmatrix} 0 & \frac{1}{2} & \frac{1}{2} \\ \frac{1}{2} & 1 & 0 \\ \frac{1}{2} & 0 & -1 \end{pmatrix} \Big)\}, \end{aligned} \tag{25}$$

where again, the prefactor $|Y_\nu|$ can be calculated from $|Y_{SL}|$ and M_R. Note that the flavour structure of eq. (25) differs significantly from eq. (19) for the same choice of angles, see the discussion about lepton flavour violation in the next subsection.

	Parameters	Moduli	Phases
N_Y	Y_e, Y_ν, Y_{SL}, M_R Dirac type	$4 \times n^2$	$4 \times n^2$
G	$U(n)_L \bigotimes U(n)_{\nu^c} \bigotimes U(n)_{e^c} \bigotimes U(n)_S$	$-4 \times \frac{n(n-1)}{2}$	$-4 \times \frac{n(n+1)}{2}$
G'	no LF conservation		
N_{phys}		24	12

TABLE III: Parameter counting for the linear seesaw model for three generations.

In case of the linear seesaw, loop contributions to the neutrino masses from the splitting in the sneutrino sector is always negligible for neutrino masses in the sub-eV range, assuming

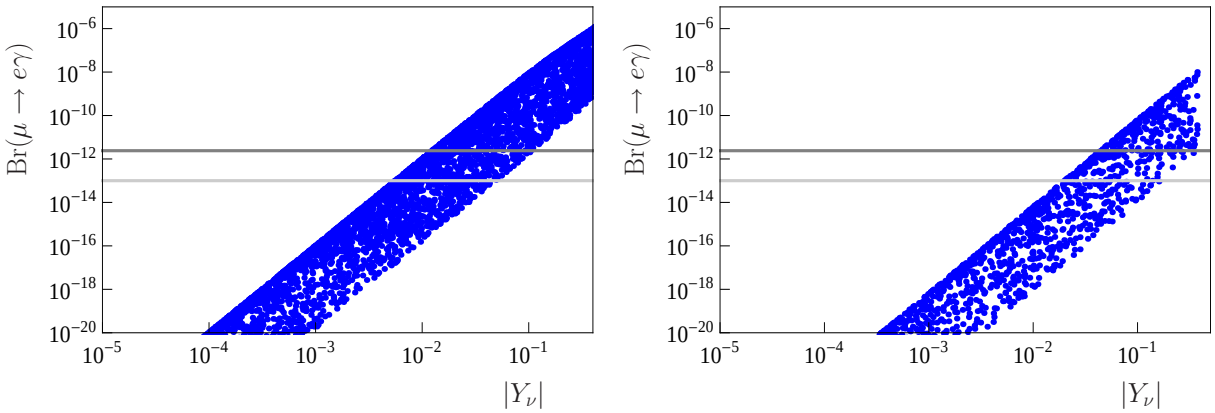

FIG. 2: $\mathrm{Br}(\mu \to e\gamma)$ calculated in the inverse (left) and linear (right) seesaw. Here, all flavour has been put into the Yukawa Y_ν, while neutrino angles have been fitted to their best fit point values [8]. A random scan over m_0 and M_R in the interval [100,1000] GeV and $B_{M_R} = [10^3, 10^6]$ GeV^2 has been performed for these points. Note that the axis are the same for inverse and linear seesaw for an easier comparison. Linear seesaw leads to smaller LFV than inverse seesaw for equal choice of neutrino angles.

the trilinears to be proportional to $T_x \propto Y_x A_0$. This can be understood as follows: The difference in the eigenvalues of the CP-even and CP-odd sector is entirely due to the different signs in the off-diagonals in eq. (9). As can be easily shown, the maximum difference in the eigenvalues is reached for $Y_{SL} \simeq Y_\nu$. However, eq.(22) shows that the product $Y_{SL}Y_\nu$ is required to be small, due to the observed smallness of neutrino masses. Thus, the splitting in the sneutrino sector in case of linear seesaw is maximally of the order of $m_\nu m_{SUSY}$, i.e. $\mathcal{O}(10^{-9})$ GeV^2.

B. Lepton flavour violation

In any supersymmetric model, limits on lepton flavour violating decays such as $\mu \to e\gamma$ provide an important constraint on the parameter space [70]. In models with a low scale seesaw especially important constraints come from $l_i \to 3l_j$ [71] and from $\mu - e$ conversion in nuclei [72].

The fit to neutrino data requires non-trivial flavour violating entries in at least one of the Yukawa- or mass matrices: Y_ν or Y_{SL} for linear and Y_ν or μ_S for inverse seesaw. If we assume

that the LFV resides in Y_ν, limits on the Yukawa result as shown in fig. (2). In this figure we have chosen μ_S (left) or Y_{SL} (right) diagonal and neutrino angles have been fitted to their best fit point values [8] using Y_ν. A random scan over m_0 and M_R in the interval [100,1000] GeV and $B_{M_R} = [10^3, 10^6]$ GeV^2 has been performed for these points, fixing $\tan\beta = 10$ and $M_{1/2} = 2.5$ TeV. Upper limits of the order of (few) 10^{-2} (10^{-1}) result for inverse (linear) seesaw, despite the heavy SUSY spectrum (due to the large value of $M_{1/2}$). Much stronger limits result for lighter spectra. Note that $l_i \to 3l_j$ [71] and $\mu - e$ conversion in nuclei [72] can lead to even stronger limits. We will not repeat this exercise here.

Note also, as discussed in the next section, that the constraints from relic density of sneutrinos lead to an approximate lower bound on the absolute size of the Yukawa coupling $|Y_\nu|$.

IV. SNEUTRINO DARK MATTER

In this section we discuss the relic abundance (RA) and the direct detection cross section (DD) of sneutrinos in the different models. We will first discuss the simpler case of the inverse/linear seesaw and then turn to the mBLR model.

In order to reduce the number of free parameters in our numerical scans, we calculate all spectra with CMSSM-like boundary conditions, i.e. at the GUT scale we choose $(m_0, M_{1/2}, A_0, \tan\beta, \mathrm{sgn}(\mu))$, from which all soft parameters at the electro-weak scale are calculated using full 2-loop RGEs. Unless noted otherwise, we always assume that the trilinear soft parameters are related to the superpotential parameters in a "mSugra"-like way: $T_\alpha \propto Y_\alpha A_0$ at m_{GUT}.

In addition to the MSSM parameters, we have the neutrino Yukawa couplings Y_ν and several model specific parameters. These are M_R and B_{M_R} and, in case of the inverse (linear) seesaw μ_S and B_{μ_S} (Y_{SL}). While, in principle, all of these are matrices we use eq. (17) and (23)) to fit neutrino data and usually assume all matrices are diagonal except one.

For the mBLR model we have the free parameters Y_s, v_R, $\tan\beta_R$, μ_R and m_{A_R}. Recall, $M_R = Y_s v_R/\sqrt{2}$ and m_{A_R} is the CP-odd scalar Higgs mass in the χ_R sector. Due to the constraints from LFV discussed above, we usually put all LFV into either μ_S (inverse seesaw) or Y_{SL} (linear seesaw). This way we only have to check for the constraints from Z^0 and Higgs physics and lower limits on squarks and gluinos discussed in section (III).

A. Inverse/Linear seesaw

Sneutrinos can be the LSP, practically independent from the actual choice of the CMSSM parameters. This can be easily understood from eqs (7) and (9) and is demonstrated by two simple examples in fig. (3).

In fig. (3) we show two examples of tree-level sneutrino masses calculated as function of B_{M_R} for two particular but arbitrary choices of parameters: $m_0 = 100$, $M_{1/2} = 1000$, $A_0 = 0$ and $\mu = 800$ all in GeV and $|Y_\nu| = 0.1$ and $\tan\beta = 10$. In addition, $M_R = 200$ GeV (left) and $M_R = 500$ GeV (right). This calculation was made in a one generation toy model and serves only for illustration. The general behaviour is easily understood. First, recall that within CMSSM roughly $m_{\chi_1^0} \sim m_{\tilde{B}} \sim 0.4 M_{1/2}$. Entries on the diagonals of the sneutrino mass matrix are of the order $m^2_{LL} \simeq m_0^2 + 0.5 M^2_{1/2}$, $m^2_{\nu^c\nu^c} \simeq m_0^2 + M_R^2$ and $m^2_{SS} \simeq m_0^2 + M_R^2$. If $\sqrt{m_0^2 + M_R^2} \lesssim 0.4 M_{1/2}$ (one of the pair of) right sneutrinos is the LSP, see left plot. On the other hand, for larger values of m_0 and or M_R, right sneutrinos still can be the LSP if $B_{M_R} \gtrsim \sqrt{m_0^2 + M_R^2}$, since in this case a large off-diagonal in the sneutrino mass matrix leads to a large splitting between the two lightest eigenstates, with the lighter one becoming very light, see right plot. Since B_{M_R} is naively expected to be of order m^2_{SUSY}, sizeable splitting between the right sneutrinos is expected and in a random scan over parameters such sneutrinos emerge as LSP quite often. Note, that a light eigenvalue in the sneutrino sector can also be made by a large off-diagonal in the sneutrino mass matrix in the LR and LS entries of the mass matrix.

In the early universe sneutrinos can annihilate into SM particles through various types of interactions. The most important Feynman diagrams are shown in figs (4) and (5). Fig. (4) shows the quartic interaction between two sneutrinos and two Higgses and s-channel Higgs exchange. The former is very efficient for $m_{\tilde{\nu}_{LSP}} \geq m_{h^0}$, while the latter is important near $m_{\tilde{\nu}_{LSP}} \simeq m_{h^0}/2$. Fig. (5) shows the quartic interaction with W- and Z-bosons and t-channel neutralino exchange. The importance of the latter depends on the SUSY spectrum.

The relative importance of different diagrams is strongly dependent on the kinematical regime. A typical example of final state branching ratios versus the lightest sneutrino mass is shown in fig (6). In this scan we have fixed $m_0 = 120$, $M_{1/2} = 600$, $A_0 = 0$ all in GeV and $|Y_\nu| = 0.4$ and $\tan\beta = 10$. In addition $\mu_S = [10^{-11}, 10^{-9}]$ GeV.

From left to right we see that the most important channels are $\tilde{\nu}_{LSP}\tilde{\nu}_{LSP} \longrightarrow \tau\overline{\tau}$ (ma-

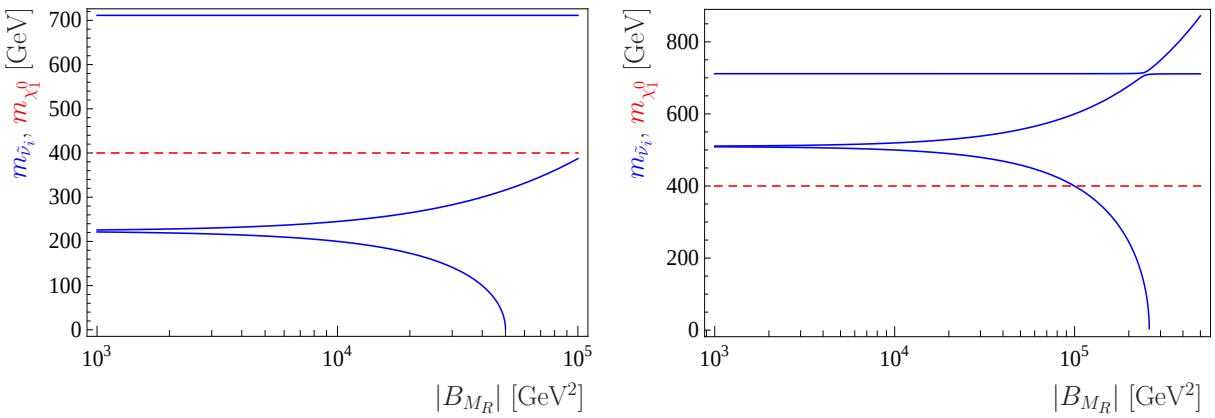

FIG. 3: Two examples of tree-level sneutrino masses calculated as function of B_{M_R} for two particular but arbitrary choices of parameters: $m_0 = 100$, $M_{1/2} = 1000$, $A_0 = 0$ and $\mu = 800$ all in GeV and $|Y_\nu| = 0.1$ and $\tan\beta = 10$. In addition $M_R = 200$ GeV (left) and $M_R = 500$ GeV (right). For comparison also the lightest neutralino mass is shown.

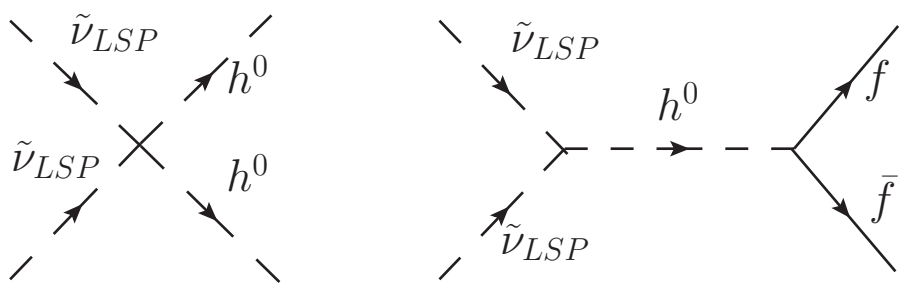

FIG. 4: Examples of Feynman diagrams contributing to the $\tilde{\nu}_{LSP}\tilde{\nu}_{LSP}$ annihilation: To the left quartic interaction; to the right s-channel Higgs exchange.

genta with triangles), $\tilde{\nu}_{LSP}\tilde{\nu}_{LSP} \longrightarrow b\bar{b}$ (brown), $\tilde{\nu}_{LSP}\tilde{\nu}_{LSP} \longrightarrow \nu\nu_R$ (orange), $\tilde{\nu}_{LSP}\tilde{\nu}_{LSP} \longrightarrow W^+W^-$ (red), $\tilde{\nu}_{LSP}\tilde{\nu}_{LSP} \longrightarrow Z^0Z^0$ (purple), $\tilde{\nu}_{LSP}\tilde{\nu}_{LSP} \longrightarrow HH$ (blue), $\tilde{\nu}_{LSP}\tilde{\nu}_{LSP} \longrightarrow t\bar{t}$ (green); finally, to the right of the figure, the contributions coming from the coannihilations are shown: $\tilde{e}\tilde{e} \longrightarrow \tau\tau$ (magenta with triangles), and $\tilde{e}\bar{\tilde{e}} \longrightarrow \gamma\gamma$ (in yellow).

For low sneutrino masses the determination of the relic abundance is dominated by Higgs exchange, see fig. (4) right. Since the Higgs couplings are proportional to SM fermion masses, $b\bar{b}$ is most important in the low mass regime, followed by $\tau\bar{\tau}$. For sneutrino masses above approximately $m_{\tilde{\nu}_{LSP}} \sim 45$ GeV the final state $\nu\nu$ becomes dominant in this example. This is because with these parameter choices the lightest of the "singlet" neutrinos has a

]

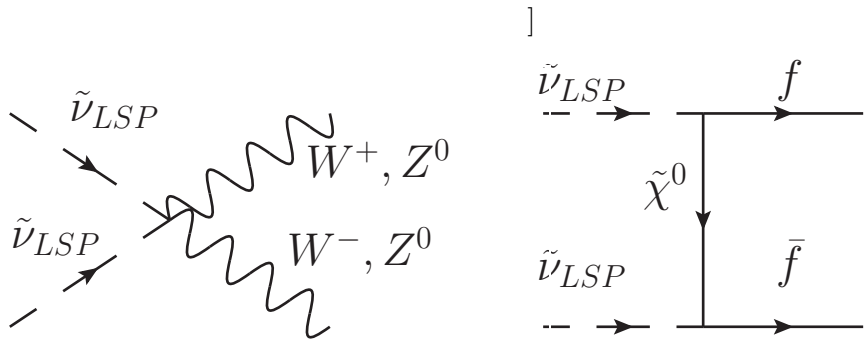

FIG. 5: Examples of Feynman diagrams contributing to the $\tilde{\nu}_{LSP}\tilde{\nu}_{LSP}$ annihilation: To the left quartic interaction with gauge bosons; to the right t-channel neutralino exchange.

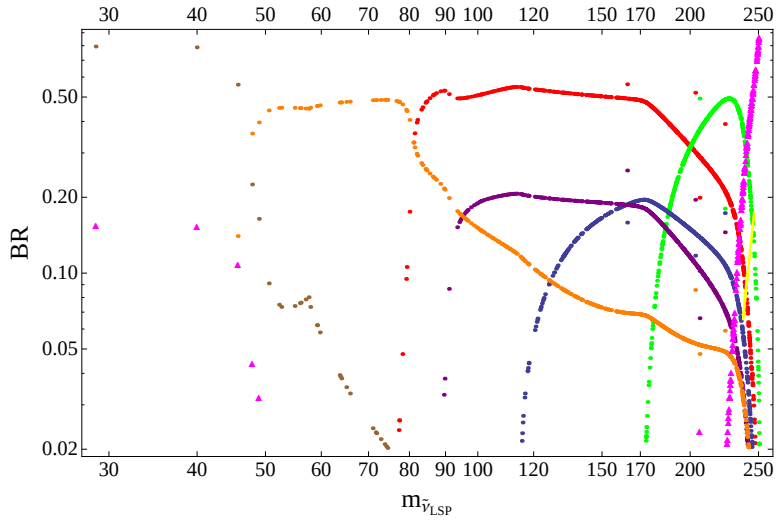

FIG. 6: Examples of final state branching ratios for the annihilation cross section of sneutrinos to SM final states versus the lightest sneutrino mass (in GeV). For the parameter choices of this scan, see text. Calculation uses the inverse seesaw model. Different kinematical regimes are visible, see discussion.

mass of about 45 GeV and the Higgs couples always to $\nu_L\nu_R$, i.e. one light and one heavy neutrino.

Single Z^0 exchange is less important than Higgs exchange, since scalar-scalar-vector couplings are momentum suppressed. For $m_{\tilde{\nu}_{LSP}} \gtrsim 80$ GeV, however, two gauge boson final states become dominant, the channel W^+W^- being more important than Z^0Z^0. For masses above $m_{\tilde{\nu}_{LSP}} \gtrsim 120$ GeV also two Higgs final states are sizable. All these final states are due to quartic interactions, see fig. (4) left and fig. (5). Due to the large top Yukawa coupling,

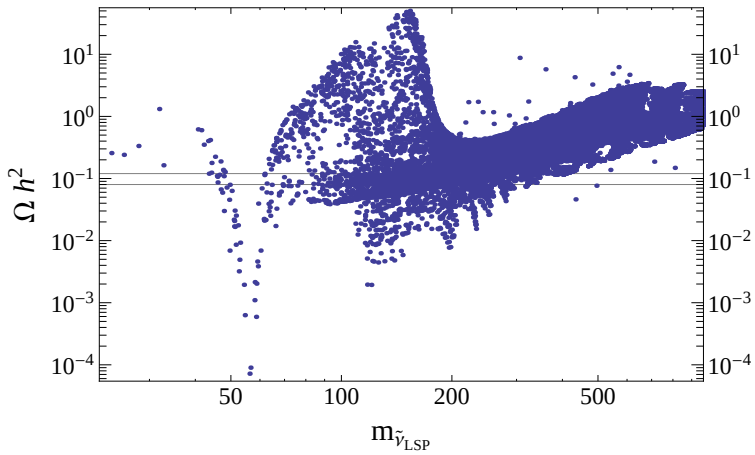

FIG. 7: General scan for the inverse seesaw model. The plot shows Ωh^2 versus the mass of the lightest sneutrino (in GeV) for points in which the sneutrino is the LSP.

the two top final state, once kinematically possible, becomes very important. And, finally, for $m_{\tilde{\nu}_{LSP}}$ approaching the NLSP mass, in this example the lightest scalar tau, coannihilation into taus becomes dominant.

Next, we have performed a general scan over the parameter space of the model choosing randomly $(m_0, M_{1/2}, A_0, \tan\beta, \mathrm{sgn}(\mu))$ in the interval $m_0 = [100, 3000]$, $M_{1/2} = [200, 3000]$, $A_0 = 0$, $\tan\beta = 10$ and $\mathrm{sgn}(\mu) > 0$ and $|Y_\nu| = 0.3$, $M_R = [0, 1000]$. B_{M_R} is calculated accordingly to enhance the percentage of sneutrino LSP points. We post-select data points with sneutrino LSPs and cut on all points not fulfilling the lower bounds on squark and gluinos masses from the LHC [61]. Results are shown in fig. (7) for the case of the inverse seesaw. Shown is the calculated RA (Ωh^2) versus the mass of the lightest sneutrino for points in which the sneutrino is the LSP. The band, which is the allowed range from WMAP [73], shows that one can easily get points with the correct relic abundance over a wide range of parameters. The figure is for the inverse seesaw, linear seesaw is qualitatively very similar.

The plot shows several distinct features. First, for masses of sneutrinos around $m_{\tilde{\nu}_{LSP}} \simeq$ 60 GeV a strong reduction of the RA occurs, due to the s-channel Higgs exchange. As can be seen, this diagram is very effective in reducing the RA whenever $m_{\tilde{\nu}_{LSP}}$ is within a few GeV of the mass of the Higgs, but less important elsewhere. In the region above $m_{\tilde{\nu}_{LSP}} = 80$ GeV, quartic interactions with the gauge bosons are effective and above $m_{\tilde{\nu}_{LSP}} = 175$ GeV two-top final states become dominant. For very large $m_{\tilde{\nu}_{LSP}}$ one sees an overall trend that the RA rises with rising sneutrino mass, apart from a few scattered points. Low RA, i.e.

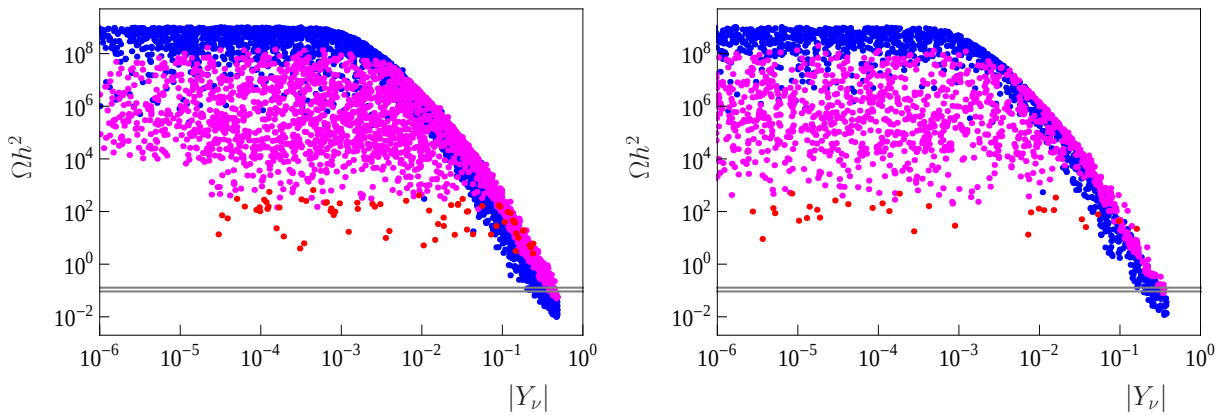

FIG. 8: Scan for the inverse (left) and linear (right) seesaw model. The plot shows Ωh^2 versus $|Y_\nu|$ in a scan over the remaining parameters, see text. The color coding of the points shows the mass difference between the lightest sneutrino mass and the NLSP (next-to-LSP) mass, in this scan practically always the lightest of the charged sleptons. Red: $m_{NLSP} - m_{LSP} < 100$ GeV, violet: $100 < m_{NLSP} - m_{LSP} < 500$ GeV, blue: $m_{NLSP} - m_{LSP} > 500$ GeV. For a discussion see text.

$\Omega h^2 \simeq 0.1$, in this high mass regime can practically only be made via co-annihilation or s-channel heavy Higgs exchange. Note that the fact that there are only a few points with $m_{\tilde{\nu}_{LSP}}$ below 50 GeV is just an artifact of the scanning procedure. However, the general trend is that for very light sneutrinos the calculated RA is larger than $\Omega h^2 \sim 0.1$. We will come back to a more detailed discussion of light sneutrinos in the next section.

In fig. (7) we have fixed the neutrino Yukawa couplings to a constant value. However, sneutrinos which are purely singlets do not couple to gauge bosons and thus their relic abundance is usually too large. For mixed sneutrinos the RA depends strongly on the choice of $|Y_\nu|$. An example is shown in fig. (8). The figure shows on the left (right) results for the inverse (linear) seesaw. In both cases we have fitted neutrino data, using eqs (17) and (23), and scanned over the parameters: m_0 and M_R in the interval [100,1000] GeV and $B_{M_R} = [10^3, 10^6]$ GeV^2. Here, $M_{1/2}$ was fixed to $M_{1/2} = 2.5$ TeV and $\tan\beta = 10$ and $A_0 = 0$. The choice of such a large $M_{1/2}$ guarantees that all points have a lightest Higgs mass in the vicinity of 125 GeV. It also makes all SUSY particles, except the sneutrino, relatively heavy.

The points in fig. (8) are color coded by the mass difference between the lightest sneutrino mass and the NLSP (next-to-LSP) mass, in this scan practically always the lightest of the charged sleptons. Red: $m_{NLSP} - m_{LSP} < 100$ GeV, violet: $100 < m_{NLSP} - m_{LSP} < 500$

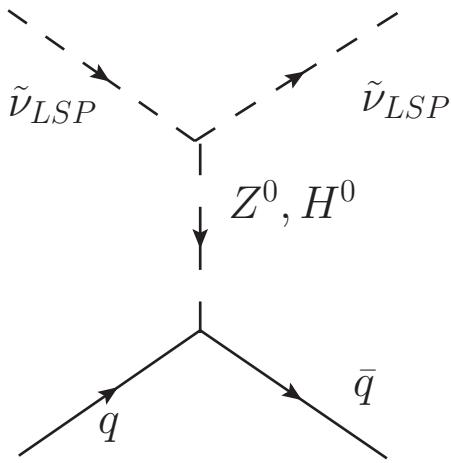

FIG. 9: Diagrams contributing to the direct detection cross section: elastic scattering of $\tilde{\nu}_{LSP}$ over quarks.

GeV, blue: $m_{NLSP} - m_{LSP} > 500$ GeV. For large $|Y_\nu|$ the RA goes down as $\Omega h^2 \propto |Y_\nu|^{-4}$, for small values of Y_ν the points show practically no dependence on $|Y_\nu|$. This is because the determination of the RA is then dominated by coannihilation processes with the lightest stau. These can be very efficient, if $\Delta m^2 = m_{\tilde{l}}^2 - m_{\tilde{\nu}_{LSP}}{}^2 \simeq$ few GeV, less so for larger mass differences. Thus, to reduce the relic density of the sneutrino to acceptably small values, one needs either a special kinematic configuration, such as co-annihilation or s-channel resonance, or $|Y_\nu|$ has to be larger than roughly $|Y_\nu| \gtrsim 0.1$.

1. *Direct Detection*

Direct detection of the sneutrinos consists in detecting the recoil energy coming from the elastic scattering of sneutrinos with nuclei inside a detector. The interaction, which occurs in the non relativistic limit, since the velocity of dark matter particles in the Galactic halo is small, comes from basically two diagrams contributing at tree level: the t-channel exchange of a neutral Higgs or of the Z boson. Which of the two diagrams is the more important one depends on the actual value of $|Y_\nu|$.

The Z–boson exchange cross section is [30]:

$$\sigma^Z_{\tilde{\nu}_{LSP}\,\mathcal{N}} = \frac{G_F^2}{2\pi} \frac{m^2_{\tilde{\nu}_{LSP}} m^2_{\mathcal{N}}}{(m_{\tilde{\nu}_{LSP}} + m_{\mathcal{N}})^2} \left[A_{\mathcal{N}} + 2(2\sin^2\theta_W - 1)Z_{\mathcal{N}}\right]^2 \tag{26}$$

where $m_{\mathcal{N}}$ is the nucleus mass, $A_{\mathcal{N}}$ and $Z_{\mathcal{N}}$ are the mass number and proton number of the

nucleus and G_F is the Fermi constant.

The Higgs–bosons exchange scattering cross section is [30]:

$$\sigma^{Higgs}_{\tilde{\nu}_{LSP}\mathcal{N}} = \frac{m_p^2}{4\pi(m_{\tilde{\nu}_{LSP}} + m_{\mathcal{N}})^2}\left[f_p Z_{\mathcal{N}} + f_n\left(A_{\mathcal{N}} - Z_{\mathcal{N}}\right)\right]^2 \tag{27}$$

where $\mathcal{N}$ denotes the nucleus, and the quantities $A_{\mathcal{N}}$ and $Z_{\mathcal{N}}$ are the mass number and proton number of the nucleus, f_p and f_n are hadronic matrix elements which parametrize the quark composition of the proton and the neutron, and which represent the effective coupling of the $\tilde{\nu}_{LSP}$ to the nucleus, but are subject to considerable uncertanties [30, 75].

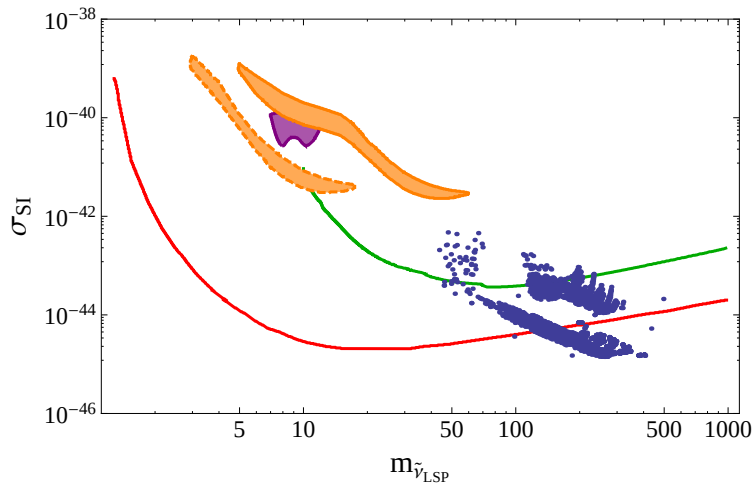

FIG. 10: Direct detection cross section (in $[cm^2]$) for sneutrino LSPs (masses in GeV), for the inverse seesaw model. The points are those from fig. (7) compatible with the upper bound on the relic abundance. Also the current limits from XENON-100 [74] (red line), CDMS [76] (green line), DAMA (with and without channeling, orange regions) [77], and Cogent [78] (purple region) are shown for comparison.

In figure (10) we depict the direct detection cross section versus the LSP sneutrino mass (blue points). The points are the same as shown in fig. (7), but after a cut on the relic abundance. In the same plot, the current limits from XENON-100 [74] (red line), CDMS [76] (green line), DAMA (with and without channeling, orange regions) [77], and Cogent [78] (purple region) are shown. The major bound nowadays comes from the XENON-100 experiment [74], whose best sensitivity is around 10^{-44}cm^2 for a dark matter candidate of 50 GeV. The sneutrinos show a SI cross section $\sigma_{SI} \lesssim 10^{-42}$cm^2, and for masses $m_{\tilde{\nu}_{LSP}} \gtrsim 100$ GeV they are compatible with current limits by XENON-100. However, XENON-1T, whose sensibility should improve up to 10^{-46}cm^2, will test those cross sections.

We have not been able to find low sneutrino masses of the order of $\mathcal{O}(5-10)$ GeV, which have the correct relic density and fulfill at the same time the constraints from the direct detection experiment XENON-100 [74]. However, this calculation has been done with $B_{\mu_S} \propto m_0 \mu_S$ and lepton number violation in the sneutrino mass matrix leads to the mass splitting between the real and the imaginary part of the lightest sneutrino, and the scattering via Z boson exchange occurs inelastically, through a transition from the real to the imaginary or viceversa. Points shown in fig. (10) have all very small splitting in the sneutrino sector, but if the mass splitting is greater than some keV, scattering is strongly suppressed at direct detection experiments. Indeed, the maximum kinetic energy that the sneutrino LSP can transfer to the detector depends on the velocity it moves relative to the nucleus v ($\simeq 10^{-3}$ in the galactic halo),the nucleus mass M and the angle θ of scattering:

$$E = \frac{A^2 v^2}{M}(1 - cos(\theta)) \tag{28}$$

where $A = \frac{m_{\tilde{\nu}_{LSP}} M}{m_{\tilde{\nu}_{LSP}} + M}$, which would give, in the case of a Xenon detector for instance, and $m_{\tilde{\nu}_{LSP}} = 100$ GeV, E = 25 keV (if $\cos(\theta) = 0$). For heavier sneutrinos with a mass of the order of TeV, for a splitting larger than some hundred keV the direct detection cross section goes to zero. Such "large" splitting is currently not excluded in the inverse seesaw, compare to fig. (1). Thus, in principle inverse seesaw can evade all constraints from direct detection, while linear seesaw can not, see the discussion in section (III A 2).

B. mBLR model

In this subsection we discuss the DM phenomenology of the supersymmetric $U(1)_R \times U(1)_{B-L}$ extension of the standard model. The main difference to the simpler models discussed previously are the presence of the extra gauge boson Z' and the possibility to have an additional light, mostly singlet Higgs boson, which lead to some important changes in the phenomenology.

First, recall that the $U(1)_R \times U(1)_{B-L}$ gauge symmetry of this model is spontaneously broken to the hypercharge group $U(1)_Y$ by the vevs v_{χ_R} and $v_{\bar{\chi}_R}$ of the scalar components of the $\hat{\chi}_R$ and $\hat{\bar{\chi}}_R$ superfields whereas the $SU(2)_L \otimes U(1)_Y \to U(1)_Q$ breaking is driven by the vevs v_d and v_u of the neutral scalar components of the $SU(2)_L$ Higgs doublets H_d and H_u up to gauge kinetic mixing effects. The tadpole equations for the different vevs can be solved

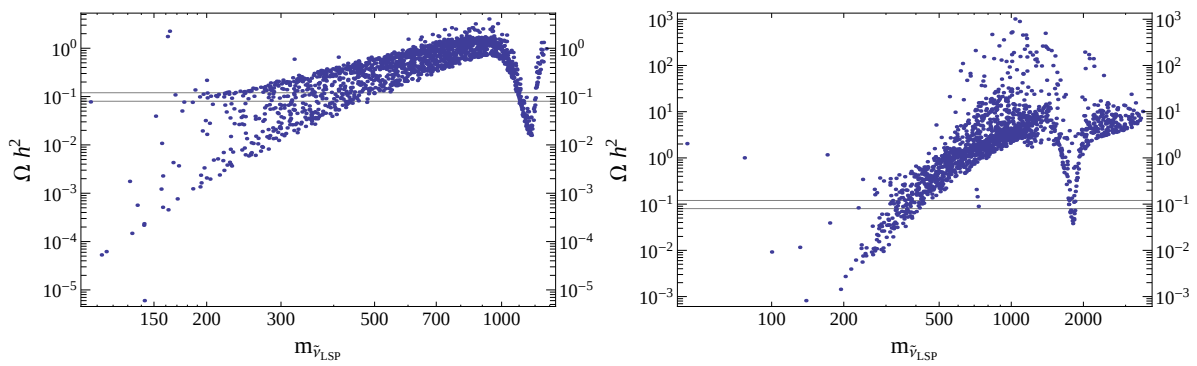

FIG. 11: Scan for the CmBLR version of the extended gauge model. Parameters are varied as follows: $m_0 = [0, 6000]$ GeV, $M_{1/2} = [3000, 8000]$ GeV, $\tan\beta_R = [1.0,1.3]$. The other parameters are set to the values $\tan\beta$=10, $A_0 = -4500$ GeV, $Y_S = \mathrm{diag}(0.3)$; v_R has been chosen different in the two plots, $v_R = 6$ TeV and $v_R = 10$ TeV, respectively. Masses of the $\tilde{\nu}_{LSP}$ are in GeV.

analytically for either (i) (μ, B_μ, μ_R, B_{μ_R}) or (ii) (μ, B_μ, $m^2_{\chi_R}$,$m^2_{\bar{\chi}_R}$) or (iii) ($m^2_{H_d}$, $m^2_{H_u}$, $m^2_{\chi_R}$, $m^2_{\bar{\chi}_R}$) [13].

We address the minimal version option (i) as CmBLR (constrained mBLR), since it allows to define boundary conditions for all scalar soft masses at m_{GUT}, reducing the number of free parameters by four, although leading to some constraints on the parameter space, such as a lower bound on $\tan\beta_R$ ($\tan\beta_R > 1$) [13]. The second option (ii) is instead more flexible, and we have made use of it in some of our scans, too. We will refer to this option as χ_RmBLR version (non-universal χ_R masses mBLR). We have not used the last option, which we only mentioned for the sake of completeness.

The result of Ωh^2 for two general scans is shown in fig. (11). Parameters have been scanned as described in the figure caption. Note that there are two fixed but different choices of v_R in the left and right plots, leading to two different values of the Z' mass. In both plots in fig. (11) the main feature clearly visible is the Z' pole. Indeed, the annihilation of the $\tilde{\nu}_{LSP}$ LSPs into SM particles via the Z' becomes efficient when the mass of the $\tilde{\nu}_{LSP}$ is close to half the mass of the Z'. The mass of the Z' can be calculated analytically [13] and mainly depends on the value of v_R, see eq.(13). The ATLAS searches for a Z' set a lower limit on its mass which is 1.8 TeV, and this translates into a lower limit on $v_R \gtrsim 5$ TeV, see the plot on the left. The plot on the right shows that choosing a higher value of v_R we can get very heavy $\tilde{\nu}_{LSP}$ DM with the correct RA, up to masses of several TeV.

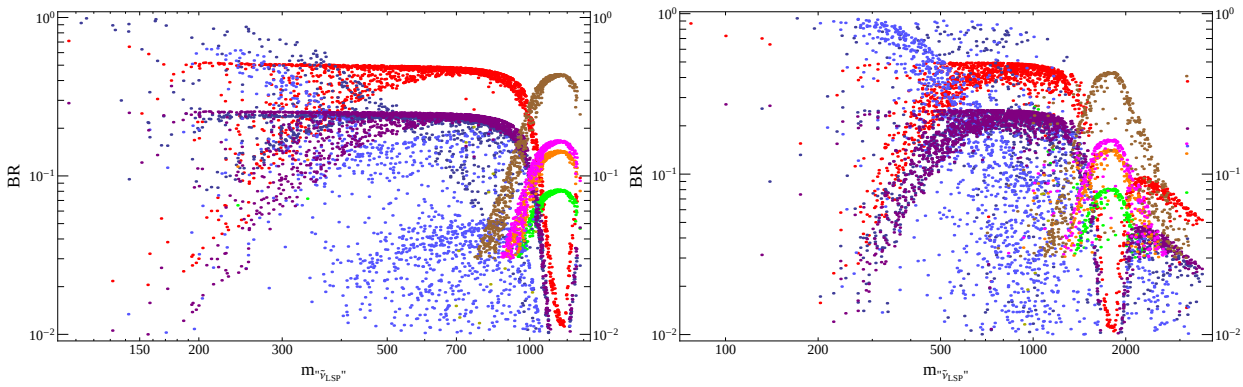

FIG. 12: Final state branching ratios for the annihilation cross section of sneutrinos to SM final states versus the lightest sneutrino mass (in GeV). For the parameter choices of these scans see fig. (11). For a discussion of the different kinematical regimes which are visible, see text.

The main annihilation channels for sneutrino DM for the points of fig. (11) are shown in fig. (12). Far from the Z'-pole resonance these are $\tilde{\nu}_{LSP}\tilde{\nu}_{LSP} \longrightarrow \tau\overline{\tau}$ (magenta), $\tilde{\nu}_{LSP}\tilde{\nu}_{LSP} \longrightarrow b\overline{b}$ (brown), $\tilde{\nu}_{LSP}\tilde{\nu}_{LSP} \longrightarrow \nu\nu_R$ (orange), $\tilde{\nu}_{LSP}\tilde{\nu}_{LSP} \longrightarrow W^+W^-$ (red), $\tilde{\nu}_{LSP}\tilde{\nu}_{LSP} \longrightarrow Z^0Z^0/Z_RZ_R$ (purple), $\tilde{\nu}_{LSP}\tilde{\nu}_{LSP} \longrightarrow HH$ (blue), $\tilde{\nu}_{LSP}\tilde{\nu}_{LSP} \longrightarrow t\overline{t}$ (green). The quartic coupling with two Higgses (h^0, h^0_{BLR} and A^0, depending on if they are kinematically allowed, depending on the $\tilde{\nu}_{LSP}$ mass) is one of the most efficients, as before. For lower masses the annihilation via the MSSM Higgs is the most efficient, as can be noticed by the small relic density for lower masses, expecially in the first plot, where on the left end side we are approaching the region where the quartic Higgs coupling is important (for $m_{\tilde{\nu}_{LSP}} \simeq 120$ GeV).

Recall that in this model the Higgs sector is more complicated due to the extended gauge structure. The $U(1)_{B-L} \times U(1)_R$ breaking results in one additional light Higgs, h^0_{BLR} [12]. The mixing between the MSSM Higgs h^0 and the h^0_{BLR} enhances the mass of the mostly MSSM Higgs, leading to a MSSM-like Higgs in accord with the most recent ATLAS and CMS preferred regions, without much constraints on the SUSY spectrum. However, this enhancement of the MSSM Higgs mass occurs usually in the model if the h^0_{BLR} has a mass of the order of the MSSM-like state or less, i.e. the presence of a light singlet Higgs is preferred unless the SUSY spectrum is rather heavy (in which case the CMSSM limit is reached).

We have also checked for constraints coming from direct detection in the limit of negligible

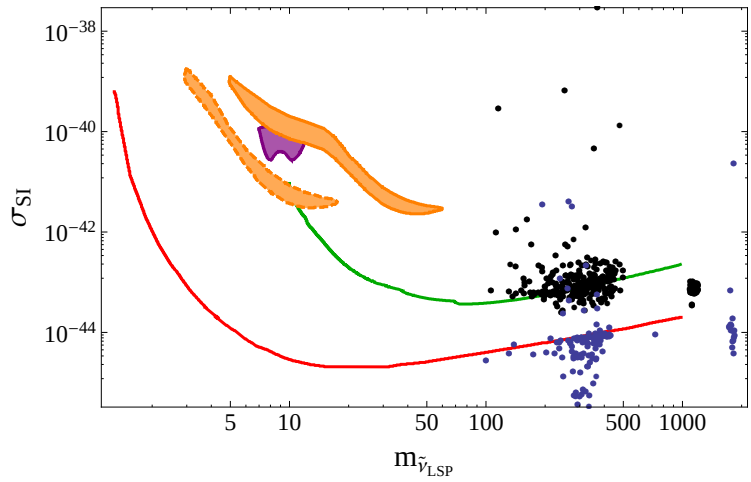

FIG. 13: Direct detection cross section (in cm^2) for sneutrino LSPs in the BLR model. Masses are in GeV. Black points refer to the scan described in fig.(11) left with $v_R = 6$ TeV. Blue points stand for the scan of fig.(11) right with $v_R = 10$ TeV. All points shown fulfill the RA constraints. Higher v_R leads in general to lower DD cross section.

sneutrino splitting. Examples for direct detection cross section are shown in fig. (13). As before, see fig.(10), different experimental constraint are also shown. All points shown fulfill the constraints from relic abundance. We have calculated two scans, one with $v_R = 6$ TeV (black) and one with $v_R = 10$ TeV (blue). As can be seen, practically all of the points with $v_R = 6$ TeV in this scan are excluded by the limit from XENON-100, while most of the $v_R = 10$ TeV are allowed. Thus XENON-100 puts currently a lower bound on v_R (and thus the Z' mass) of the order of $v_R \simeq 10$ TeV for sneutrino LSPs as DM.

The origin of this surprisingly strong constraints lies in the $Z^0 - Z'$ mixing. The mixing angle between these two states is roughly of the order $\theta_{Z^0 Z'} \sim (g_L v^2)/(g_R v_R^2)$. Thus the right sneutrinos, which couple mostly to the Z', couple via this mixing also to the Z^0. The Z^0 has an experimentally fixed mass. Thus, the only possibility to suppress the DD cross section [4] is to increase v_R.

Finally, fig. (14) shows a dedicated scan for low mass sneutrinos in the mBLR model. The different curves are slight variations of the parameters near the study point BLRSP1. The original parameters of BLRSP1 were: $m_0 = 470$, $M_{1/2} = 700$, $\tan\beta = 20$, $A_0 = 0$, $v_R = 4700$,

[4] Apart from a large sneutrino splitting.

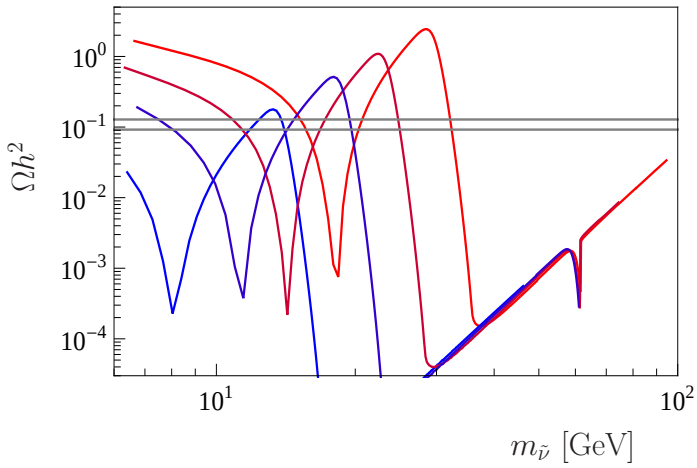

FIG. 14: Scan into the low sneutrino mass region using the mBLR model. For the parameter choices see text. The figure demonstrates that the mBLR mode can give the correct RA for low mass sneutrinos in those parts of the parameter space where a light, singlet Higgs is present.

$\tan\beta_R = 1.05$, $\mu_R = -1650$ and $M_{A_R} = 4800$ GeV. To obtain very light sneutrinos, m_0 has been lowered to $m_0 = 440$ GeV, while the different curves are for $M_{1/2} = 650, 660, 675$ and 700 GeV and the scanning runs m_{A_R} from $3000 - 4000$ GeV. The resulting scan produces sneutrinos with masses in the interval $[5, 100]$ GeV, while the lightest Higgs mass, in this case a mostly singlet Higgs, has a mass eigenvalues of $m_{h_1} \simeq 1 - 50$ GeV. The figure shows a pole around $m_{\tilde{\nu}_{LSP}} \simeq 62$ GeV, due to a mass for the MSSM-like Higgs of around $124 - 125$ GeV in all cases. There appear additional dips in the RA for smaller sneutrino masses, whenever $m_{\tilde{\nu}_{LSP}} \simeq m_{h_1}/2$. This demonstrates that in the extended gauge model it is possible to have the correct RA even for very low sneutrino masses.

However, note that, while the model can in principle give DD cross section large enough to explain the DAMA [77], and Cogent [78] hints, such points will always be inconsistent with the constraints from XENON-100 [74], also for the case of inelastic dark matter [79].

V. CONCLUSIONS

We have studied low scale seesaw models with a sneutrino LSP. We considered two possibilities: Models with the MSSM gauge group and either a linear or inverse seesaw and a model with the gauge group $SU(3)_c \times SU(2)_L \times U(1)_{B-L} \times U(1)_R$ and an inverse seesaw.

Sneutrinos can be the DM in both cases, fulfilling all known experimental bounds.

However, while inverse and linear seesaw lead to different results for LFV, in general, they give similar DM results. There are some differences in detail, though: In the inverse seesaw it is possible to avoid all direct detection constraints using a large enough splitting in the sneutrino sector, which leads to "inelastic" dark matter. This is not possible in the linear seesaw, due to constraints from neutrino physics.

In the extended gauge model there is more freedom than in the simpler MSSM-group based models. Especially very light ($\mathcal{O}(1)$ GeV) or very heavy ($\mathcal{O}$(several) TeV) sneutrinos can give the correct relic density, due to the existence of a mostly singlet Higgs in the former case and due to the Z' in the latter. Very light sneutrinos could explain the hints from DAMA [77] or Cogent [78], but are inconsistent then with XENON-100 [74, 79].

Finally, it is interesting to note that in the limit of small sneutrino mass splitting the DD limit from XENON-100 [74] leads to a lower limit on v_R of the order of $\mathcal{O}(10)$ TeV for sneutrino LSPs as the dominant component of the galactic dark matter.

Acknowledgements

We thank Werner Porod and Florian Staub for helpful discussions and assistance with SPheno and SARAH. We acknowledge support from the Spanish MICINN grants FPA2011-22975, MULTIDARK CSD2009-00064 and by the Generalitat Valenciana grant Prometeo/2009/091 and the EU Network grant UNILHC PITN-GA-2009-237920.

---

[1] G. Bertone, D. Hooper and J. Silk, Phys. Rept. **405**, 279 (2005) [hep-ph/0404175].

[2] G. Jungman, M. Kamionkowski and K. Griest, Phys. Rept. **267**, 195 (1996) [hep-ph/9506380].

[3] L. E. Ibanez, *Phys. Lett.* **B137** (1984) 160.

[4] J. S. Hagelin, G. L. Kane and S. Raby, Nucl. Phys. B **241**, 638 (1984).

[5] K. Freese, *Phys. Lett.* **B167** (1986) 295.

[6] T. Falk, K. A. Olive, and M. Srednicki, *Phys. Lett.* **B339** (1994) 248–251, [hep-ph/9409270].

[7] M. W. Goodman and E. Witten, *Phys. Rev.* **D31** (1985) 3059.

[8] D. V. Forero, M. Tortola and J. W. F. Valle, arXiv:1205.4018 [hep-ph].

[9] R. Mohapatra and J. Valle, Phys. Rev. **D34**, 1642 (1986).

[10] E. K. Akhmedov, M. Lindner, E. Schnapka and J. W. F. Valle, Phys. Rev. D **53**, 2752 (1996) [hep-ph/9509255].

[11] E. K. Akhmedov, M. Lindner, E. Schnapka and J. W. F. Valle, Phys. Lett. B **368**, 270 (1996) [hep-ph/9507275].

[12] M. Hirsch, M. Malinsky, W. Porod, L. Reichert and F. Staub, JHEP **1202**, 084 (2012) [arXiv:1110.3037 [hep-ph]].

[13] M. Hirsch, W. Porod, L. Reichert and F. Staub, arXiv:1206.3516 [hep-ph].

[14] T. Asaka, K. Ishiwata and T. Moroi, Phys. Rev. D **73**, 051301 (2006) [hep-ph/0512118].

[15] T. Asaka, K. Ishiwata and T. Moroi, Phys. Rev. D **75**, 065001 (2007) [hep-ph/0612211].

[16] K. -Y. Choi and O. Seto, arXiv:1205.3276 [hep-ph].

[17] C. Weniger, JCAP **1208**, 007 (2012) [arXiv:1204.2797 [hep-ph]].

[18] S. Gopalakrishna, A. de Gouvea and W. Porod, JCAP **0605**, 005 (2006) [hep-ph/0602027].

[19] F. Borzumati and Y. Nomura, Phys. Rev. D **64**, 053005 (2001) [hep-ph/0007018].

[20] Z. Thomas, D. Tucker-Smith and N. Weiner, Phys. Rev. D **77**, 115015 (2008) [arXiv:0712.4146 [hep-ph]].

[21] B. Dumont, G. Belanger, S. Fichet, S. Kraml and T. Schwetz, arXiv:1206.1521 [hep-ph].

[22] G. Belanger, M. Kakizaki, E. K. Park, S. Kraml and A. Pukhov, JCAP **1011**, 017 (2010) [arXiv:1008.0580 [hep-ph]].

[23] G. Belanger, S. Kraml and A. Lessa, JHEP **1107**, 083 (2011) [arXiv:1105.4878 [hep-ph]].

[24] H. -S. Lee, K. T. Matchev and S. Nasri, Phys. Rev. D **76**, 041302 (2007) [hep-ph/0702223 [HEP-PH]].

[25] G. Belanger, J. Da Silva and A. Pukhov, JCAP **1112**, 014 (2011) [arXiv:1110.2414 [hep-ph]].

[26] P. Minkowski, Phys. Lett. B **67** (1977) 421.

[27] T. Yanagida, in *KEK lectures*, ed. O. Sawada and A. Sugamoto, KEK, 1979; M Gell-Mann, P Ramond, R. Slansky, in *Supergravity*, ed. P. van Niewenhuizen and D. Freedman (North Holland, 1979).

[28] R. N. Mohapatra and G. Senjanovic, Phys. Rev. Lett. **44** (1980) 912.

[29] J. Schechter and J. W. F. Valle, Phys. Rev. D **22**, 2227 (1980).

[30] C. Arina and N. Fornengo, JHEP **0711**, 029 (2007) [arXiv:0709.4477 [hep-ph]].

[31] P. Bandyopadhyay, E. J. Chun and J. -C. Park, JHEP **1106**, 129 (2011) [arXiv:1105.1652 [hep-ph]].

[32] D. G. Cerdeno and O. Seto, JCAP **0908**, 032 (2009) [arXiv:0903.4677 [hep-ph]].

[33] D. G. Cerdeno, J. -H. Huh, M. Peiro and O. Seto, JCAP **1111**, 027 (2011) [arXiv:1108.0978 [hep-ph]].

[34] C. Arina, F. Bazzocchi, N. Fornengo, J. C. Romao and J. W. F. Valle, Phys. Rev. Lett. **101**, 161802 (2008) [arXiv:0806.3225 [hep-ph]].

[35] P. S. B. Dev, S. Mondal, B. Mukhopadhyaya and S. Roy, arXiv:1207.6542 [hep-ph].

[36] H. An, P. S. B. Dev, Y. Cai and R. N. Mohapatra, Phys. Rev. Lett. **108**, 081806 (2012) [arXiv:1110.1366 [hep-ph]].

[37] S. Khalil, H. Okada and T. Toma, JHEP **1107**, 026 (2011) [arXiv:1102.4249 [hep-ph]].

[38] L. Basso, B. O'Leary, W. Porod and F. Staub, arXiv:1207.0507 [hep-ph].

[39] V. De Romeri, arXiv:1209.1465 [hep-ph].

[40] W. Porod, Comput. Phys. Commun. **153** (2003) 275 [arXiv:hep-ph/0301101].

[41] W. Porod and F. Staub, arXiv:1104.1573 [hep-ph].

[42] F. Staub, arXiv:0806.0538 [hep-ph].

[43] F. Staub, arXiv:0909.2863 [hep-ph].

[44] F. Staub, Comput. Phys. Commun. **182** (2011) 808 [arXiv:1002.0840 [hep-ph]].

[45] G. Belanger, F. Boudjema, A. Pukhov and A. Semenov, Comput. Phys. Commun. **176**, 367 (2007) [arXiv:hep-ph/0607059].

[46] G. Belanger, N. D. Christensen, A. Pukhov and A. Semenov, Comput. Phys. Commun. **182**, 763 (2011) [arXiv:1008.0181 [hep-ph]].

[47] F. Staub, T. Ohl, W. Porod and C. Speckner, Comput. Phys. Commun. **183**, 2165 (2012) [arXiv:1109.5147 [hep-ph]].

[48] M. Hirsch, H. V. Klapdor-Kleingrothaus, and S. G. Kovalenko, *Phys. Lett.* **B398** (1997) 311–314, [arXiv:hep-ph/9701253].

[49] Y. Grossman and H. E. Haber, *Phys. Rev. Lett.* **78** (1997) 3438–3441, [arXiv:hep-ph/9702421].

[50] M. Malinsky, J. C. Romao and J. W. F. Valle, Phys. Rev. Lett. **95**, 161801 (2005) [hep-ph/0506296].

[51] P. S. B. Dev and R. N. Mohapatra, Phys. Rev. D **81** (2010) 013001 [arXiv:0910.3924 [hep-ph]].

[52] V. De Romeri, M. Hirsch and M. Malinsky, Phys. Rev. D **84**, 053012 (2011) [arXiv:1107.3412 [hep-ph]].

[53] G. Aad *et al.* [ATLAS Collaboration], Phys. Lett. B **716**, 1 (2012) [arXiv:1207.7214 [hep-ex]].

[54] S. Chatrchyan *et al.* [CMS Collaboration], Phys. Lett. B **716**, 30 (2012) [arXiv:1207.7235 [hep-ex]].

[55] OPAL Collaboration, M.Z. Akrawy et. al., Phys. Lett. **B 247** (1990) 448; L3 Collaboration, O. Adriani *et al.*, Phys. Lett. **B 295** (1992) 371; DELPHI Collaboration, P. Abreu *et al.*, Z. Phys. **C 74** (1997) 57.

[56] P. Achard *et al.* [L3 Collaboration], Phys. Lett. B **517**, 67 (2001) [hep-ex/0107014].

[57] J. Beringer *et al.* [Particle Data Group Collaboration], Phys. Rev. D **86**, 010001 (2012).

[58] P. S. Bhupal Dev, Roberto Franceschini, R. N. Mohapatra, Bounds on TeV Seesaw Models from LHC Higgs Data arXiv:1207.2756

[59] CMS collaboration; PAS EXO-12015, see https://twiki.cern.ch/twiki/bin/view/CMSPublic/PhysicsResultsEX

[60] G. Aad *et al.* [ATLAS Collaboration], arXiv:1209.2535 [hep-ex].

[61] ATLAS collaboration; ATLAS-CONF-2012-109; presented at 20th International Conference on Supersymmetry and Unification of Fundamental Interactions, Peking Univ., Beijing, China, 13 - 18 Aug 2012

[62] CMS collaboration; CMS-PAS-SUS-11-016, see updates at https://twiki.cern.ch/twiki/bin/view/CMSPublic/PhysicsResultsSUS

[63] A. Santamaria, Phys. Lett. B **305**, 90 (1993) [hep-ph/9302301].

[64] J. A. Casas and A. Ibarra, Nucl. Phys. B **618**, 171 (2001) [hep-ph/0103065].

[65] D. V. Forero, S. Morisi, M. Tortola and J. W. F. Valle, JHEP **1109**, 142 (2011) [arXiv:1107.6009 [hep-ph]].

[66] F. P. An *et al.* [DAYA-BAY Collaboration], Phys. Rev. Lett. **108**, 171803 (2012) [arXiv:1203.1669 [hep-ex]].

[67] J. K. Ahn *et al.* [RENO Collaboration], Phys. Rev. Lett. **108**, 191802 (2012) [arXiv:1204.0626 [hep-ex]].

[68] P. F. Harrison, D. H. Perkins and W. G. Scott, Phys. Lett. **B530**, 167 (2002), [hep-ph/0202074].

[69] M. Hirsch, T. Kernreiter, J. C. Romao and A. Villanova del Moral, JHEP **1001**, 103 (2010) [arXiv:0910.2435 [hep-ph]].

[70] F. Borzumati and A. Masiero, Phys. Rev. Lett. **57**, 961 (1986).

[71] M. Hirsch, F. Staub and A. Vicente, Phys. Rev. D **85**, 113013 (2012) [arXiv:1202.1825 [hep-ph]].

[72] A. Abada, D. Das, A. Vicente and C. Weiland, arXiv:1206.6497 [hep-ph].

[73] D. Larson, J. Dunkley, G. Hinshaw, E. Komatsu, M. R. Nolta, C. L. Bennett, B. Gold and M. Halpern *et al.*, Astrophys. J. Suppl. **192**, 16 (2011) [arXiv:1001.4635 [astro-ph.CO]].

[74] E. Aprile, M. Alfonsi, K. Arisaka, F. Arneodo, C. Balan, L. Baudis, A. Behrens and P. Beltrame *et al.*, arXiv:1207.3458 [astro-ph.IM].

[75] A. Bottino, F. Donato, N. Fornengo and S. Scopel, Astropart. Phys. **18**, 205 (2002) [hep-ph/0111229].

[76] Z. Ahmed *et al.* [CDMS-II Collaboration], Science **327**, 1619 (2010) [arXiv:0912.3592 [astro-ph.CO]].

[77] R. Bernabei *et al.* [DAMA and LIBRA Collaborations], Eur. Phys. J. C **67**, 39 (2010) [arXiv:1002.1028 [astro-ph.GA]].

[78] C. E. Aalseth *et al.* [CoGeNT Collaboration], Phys. Rev. Lett. **106**, 131301 (2011) [arXiv:1002.4703 [astro-ph.CO]].

[79] E. Aprile *et al.* [XENON100 Collaboration], Phys. Rev. D **84**, 061101 (2011) [arXiv:1104.3121 [astro-ph.CO]].